2 Experimental Techniques and Equipment

The following section outlines the fundamental ideas of photoemission spectroscopy from surfaces (Section 2.1). The two beamlines at the synchrotron radiation facility BESSY and the endstation will be described in Section 2.2. Finally, the laser system and the scheme to synchronize laser and synchrotron radiation will be explained in Section 2.3.

2.1 Photoelectron Spectroscopy

Photoemission is based on the photoelectric effect and is one of the most common experimental techniques to obtain information on the electronic structure of matter. The sample is irradiated by photons, ideally from a highly monochromatic light source, and the emitted electrons are analyzed with respect to their kinetic energy and their direction of propagation in angle-resolved photoemission.

Ultraviolet photoelectron spectroscopy (UPS), where photons in the ultraviolet spectral range are used, usually explores the valence-band structure. When soft X-Rays are used for excitation, the technique is called X-ray photoelectron spectroscopy (XPS). XPS is used for core-level spectroscopy. Nowadays, the availability of synchrotron radiation gives access to a wide range of excitation energies and facilitates UPS and XPS experiments.

2.1.1 Surface Sensitivity

In photoemission experiments of solids only electrons originating from a thin surface layer of the sample are probed, so that photoemission is a surface sensitive technique. During transport through the solid, the electrons undergo elastic and inelastic scattering. Electrons which leave the sample without loosing energy by scattering carry direct information about the electronic structure.
Due to inelastic scattering, photoelectrons loose kinetic energy by mainly exciting secondary electrons and plasmons. Inelastic scattering is described by the inelastic mean free path or electron escape depth. The number of emitted electrons depends on the distance they have to travel in the solid in order to reach the surface. The

intensity $I(d)$ of the emitted electrons is given by

$$I(d) = I_o e^{-d/\lambda} \tag{2.1}$$

where I_o is proportional to number of the excited electrons. The energy dependence of λ is described by the so-called *universal mean free path curve* which is shown in Fig. 2.1. The minimum of this curve, in the range of 20 to 120 eV, the region of maximum surface sensitively. The large number of electrons which undergo inelastic scattering processes form the secondary electron background in a photoemission spectrum.

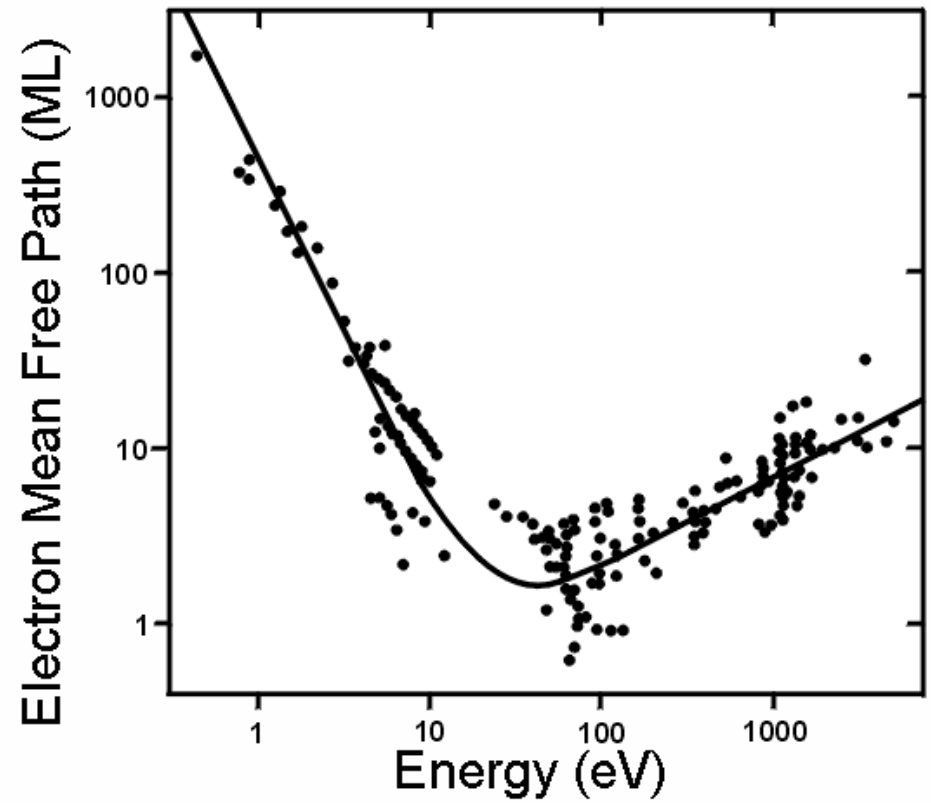

Figure 2.1: Mean free path λ in solids for electrons as a function of the kinetic energy [Ert85]. ML denotes the number of monolayers.

2.1.2 Single-Particle Picture

In the single-particle picture the conservation of energy directly relates the kinetic energy E_{kin} of the photoelectron to the photon energy $h\nu$ [Hüf95]:

$$E_{kin} = h\nu - E_B - \Phi \tag{2.2}$$

The kinetic energy of the photoelectron is usually measured with respect to the Fermi energy of the sample, E_F. E_B is the binding energy of the electron and Φ the work function of the solid (equal to the energy difference between the vacuum level and the Fermi energy). Koopman's approximation states that the binding energy measured in photoemission equals the ground-state energy of the electron that is emitted. This approximation holds only approximately and it is best for itinerant (free-electron band-like) states because it assumes that the excitation does not change any other orbital. In other words, Koopman's approximation neglects the relaxation energy.

2.1.3 Many Body Effects

The binding energy measured in photoemission is the difference between the total energy of the initial state with N electrons, E_i^N, and the final state with N-1 electrons E_f^{N-1}:

$$E_B = E_f^{N-1} - E_i^N \tag{2.3}$$

Electrons in a solid must be described by a common N-particle wave function. In addition, the photoexcitation process does not only transfer energy to the excited electron, but excites the whole N-electron system, the photohole changes the potential for the remaining N-1 electrons. The eigenstates of the system in the initial state are not identical with the eigenstates of the system after excitation. We need an additional term that describes relaxation effects:

$$E_B = h\nu - E_{kin} - \Phi - \Delta E_{relax} \tag{2.4}$$

In the valence band, a hole weakly screened by the delocalized electrons so that the relaxation energy is small. This makes photoemission a specially suited tool to investigate the valence-band structure. For localized states like core levels the relaxation energy is remarkable, due to the strong screening of the photohole.
The excited electron and the created hole are interacting with other electrons in the solid, giving rise to so-called final-state effects. The excited electron can generate secondary electrons, plasmons, and photons. The hole is screened by the remaining electrons and can decay, e.g. via Auger processes. These multielectron processes are mainly responsible for lifetime broadening, binding energy shifts, and the possible appearance of satellites lines in photoemission spectra [Hüf95].
If the system under investigation has an open shell, e.g. the gadolinium 4f core-level, with corresponding spin and angular momenta, their coupling usually lead to different final states giving rise to a rich multiplet structure; this is one reason why photoemission can be applied to investigate the magnetic properties of materials with open-shell atoms.

2.1.4 Photoemission Probability

One simplifying approach to describe the photoemission process is the so-called *three-step model* which considers the photoemission as being separable into three distinct and independent processes [Hüf95]. At first the photon is locally absorbed and an electron is excited. In the second step the electron travels through the sample to the surface and in the last step the electron escapes through the surface into the vacuum where it is detected. This separation is artificial and, in principle, the whole process of photoexcitation should be treated as a single step.
The photoexcitation probability per unit time is described by Fermi's golden rule. Most generally, the excitation process can be described as a transition of the electronic system from the initial to some final state. In the initial state, the electronic system of the solids is described by an N-electron wave function Ψ_i. After photoexcitation, the system is described by N-1 electrons remaining in the solid plus the emitted photoelectron. The photocurrent per solid angle and energy interval is [Hüf95]

$$J(\overrightarrow{k}) = \frac{k}{4\pi^2}\Sigma_i| < \Psi_f|\delta H|\Psi_i > |^2\rho(E_i + h\nu) \tag{2.5}$$

δH represents the perturbation by the electromagnetic field; ρ is the energy-dependent density of final states. The photoexcitation cross-section is strongly energy dependent.
One can determine the initial state symmetry by applying symmetry selection-rules. For normal emission, e.g, the final state wave-function in the continuum must be symmetric with respect to all symmetry operations of the surface; otherwise it will have a node at the point of the detector and no photoelectrons will be detected.

2.1.5 Sample Work Function and Kinetic Energy

Figure 2.2 shows the energy levels for a p-doped semiconductor surface and the electron distribution produced by a photon of energy hν. Upon electric contact between the sample and the analyzer the Fermi levels of both are equal. E_C, E_A, and E_V represent the energetic position of the conduction-band minimum, the acceptor, and the valence-band maximum. E_{vac} represents the vacuum energy of the analyzer and sample and $\phi_{ana/sam} = E_{vac} - E_F$ is the work function of the analyzer and the sample.
V_0 is the surface band-bending introduced, e.g, by a surface state.

The binding energy of an electron in a solid is referred to E_F, upon absorption of a photon its kinetic energy above the sample is

$$E_{kin}(sam) = h\nu - E_B - e\Phi \tag{2.6}$$

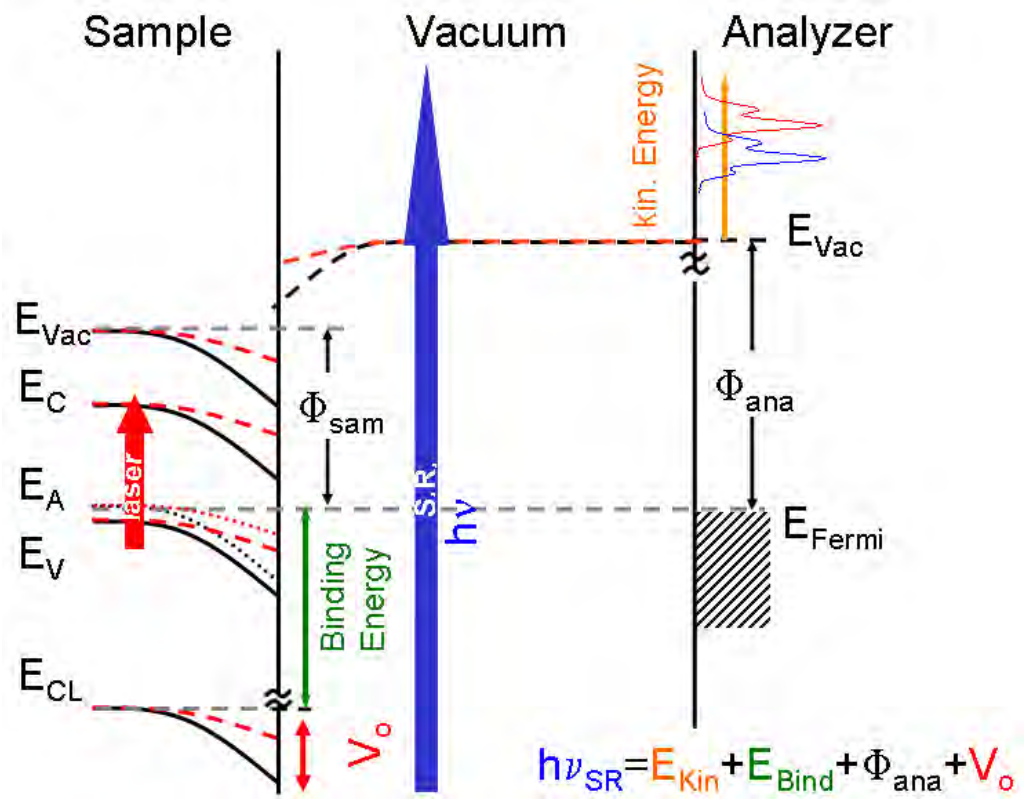

Figure 2.2: Energy levels for a semiconductor surface and the electron distribution produced by a photon of energy $\hbar\nu$ of the synchrotron radiation SR.

whereas the measured kinetic energy, as determined by the analyzer, amounts to

$$E_{kin}(ana) = h\nu - E_B - e\Phi_{ana} - V_0 \tag{2.7}$$

Therefore, the measured kinetic energy depends on the band bending and changes upon reduction of V_0, e.g, by excitation of electron-hole pairs via a laser or via the SR radiation itself.

2.1.6 Momentum Conservation in Photoemission

The photon transfers negligible momentum to the photoelectron compared to the electron momentum itself; consequently, the momentum of the photoelectron in the final state is nearly the same as in the initial state modulo a reciprocal lattice vector

$$k_f = k_i + G_B \tag{2.8}$$

k_i and k_f denote the initial-state and the final state wave-vector. These excitations are termed direct transitions and, they are represented by vertical transitions in the

reduced zone scheme .
During the escape of electrons into the vacuum (Fig. 2.3) only the parallel component of the wave-vector is conserved modulo a reciprocal surface wave vector (due to the periodicity of the lattice potential parallel to the surface). Therefore, we can connect the measured $k_{||}^{vac}$ parallel momentum with $k_{||}^{sample}$ by

$$k_{||}^{vac} = k_{||}^{sample} - G_s \tag{2.9}$$

where G_s is a reciprocal lattice vector. Photoemission processes, which involve a reciprocal lattice vector are called *umklapp* processes, and can give rise to weak usually final-state bands. Neglecting *umklapp* processes, $k_{||}^{sample}$ is expressed via the kinetic energy and the emission angle ϑ with respect to the surface normal by

$$k_{||}^{sample} = \sin\vartheta\sqrt{(\frac{2m}{\hbar^2}E_{kin})} \tag{2.10}$$

Measuring E_{kin} and ϑ in the PE experiment fixes $k_{||}^{sample}$; this is sufficient for surface states but not for bulk bands.
Variable photon energies are necessary to measure the band dispersion along a direction perpendicular to the surface. Due to the discontinuity of the potential at the surface-vacuum interface, the perpendicular component of the electron wave vector is not conserved. The expression for the component of the wave vector perpendicular to the surface is

$$k_{\perp}^{sample} = \cos\vartheta\sqrt{\frac{2m}{\hbar^2}(E_{kin} - U_0)} \tag{2.11}$$

where U_o is the inner potential of the crystal. There are several methods to determine $U_o(k_{\perp}^{sample})$ in the solid [Him78]. One can either try to identify the extrema of electron bands at the critical points and compare them with band-structure calculations. If no calculation is available, one can to first order approximate $k_{\perp}^{sample}$ by assuming free-electron-like final states, which are offset from the vacuum potential by the inner potential U_o of the crystal.

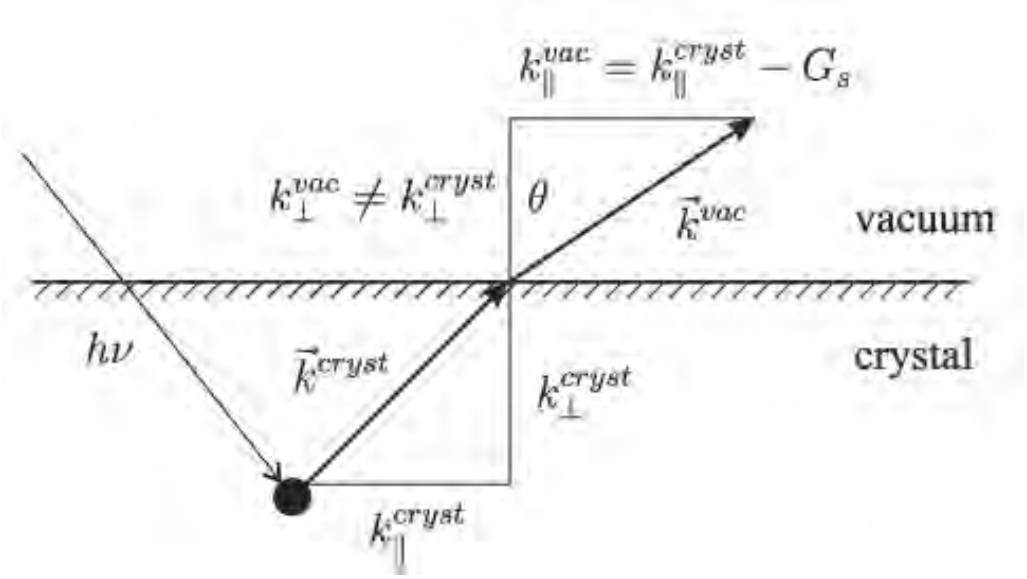

Figure 2.3: Momentum relation at the solid-vacuum interface in angle-resolved photoemission. After transmission across the crystal-vacuum interface only the parallel momentum of the photoemitted electron is conserved, but the normal component is altered by the surface potential [Hüf95].

2.2 Beamline and Endstation

The present section describes the undulator U125 beamline at the Berlin Synchrotron radiation source BESSY (Section 2.2) and the spherical grating monochromator (SGM). The endstation used at this so-called Max-Born-Institut (MBI)-BESSY beamline is outlined in Section 2.2.1. Section 2.2.3 introduces the plane grating monochromator (PGM) and Section 2.2.4 summarizes the changes made necessary upon moving the endstation to the PGM.
The working principle of the electron analyzer will be discussed in Section 2.2.5. Finally, the laser setup is described and the synchronization scheme between laser and synchrotron pulses is explained in Section 2.3.

2.2.1 Undulator U125 Beamline at BESSY II

The radiation source used for our studies is the U125 undulator, which delivers photons with energies from 15 to 600 eV depending on the position of the undulator gap and the harmonic. Synchrotron radiation (SR) is emitted when charged relativistic particles, in this case electrons, are subject to centripetal acceleration. The electrons in the BESSY storage ring have a relativistic energy of 1.7 GeV. Radiation is emitted into the forward direction within a narrow cone, tangentially to the orbit of the electrons. The opening angle of the cone (angular spread) is $\gamma^{-1} = 3,0 \cdot 10^{-4} \cong 0.02^{\circ}$.

The Undulator U125 has a wiggler design with periodic arrays of magnets located in a straight section of the storage ring. Such an array with N periods forces the electrons to move on a periodically wiggled trajectory over the length of the device [Pea97]. At each bend of the trajectories radiation is emitted in the forward direction. The intensities generated at each bend of the trajectory add up and the total intensity increases with the number of poles in the electron path. In the case of an undulator the light cones from individual wiggles overlap. This causes interference between electromagnetic waves emitted from the same electron at different positions along its travel through the device. The spectral intensity concentrates at certain wavelength. As a result quasi-monochromatic light of high brightness is obtained. The wavelength of the radiation can be varied either by changing the electron-beam energy or the undulator magnetic field strength. The magnetic field is varied by changing the undulator gap, i.e, the vertical distance between the magnets.
U125 has a horizontal linear polarization, i.e, the direction of oscillation of the electron trajectory is parallel to the plane of the floor. U125 has an overall length of 4 m with 32 periods of 125 mm. Photon fluxes obtained for 200 mA ring current are show in Fig. 2.4

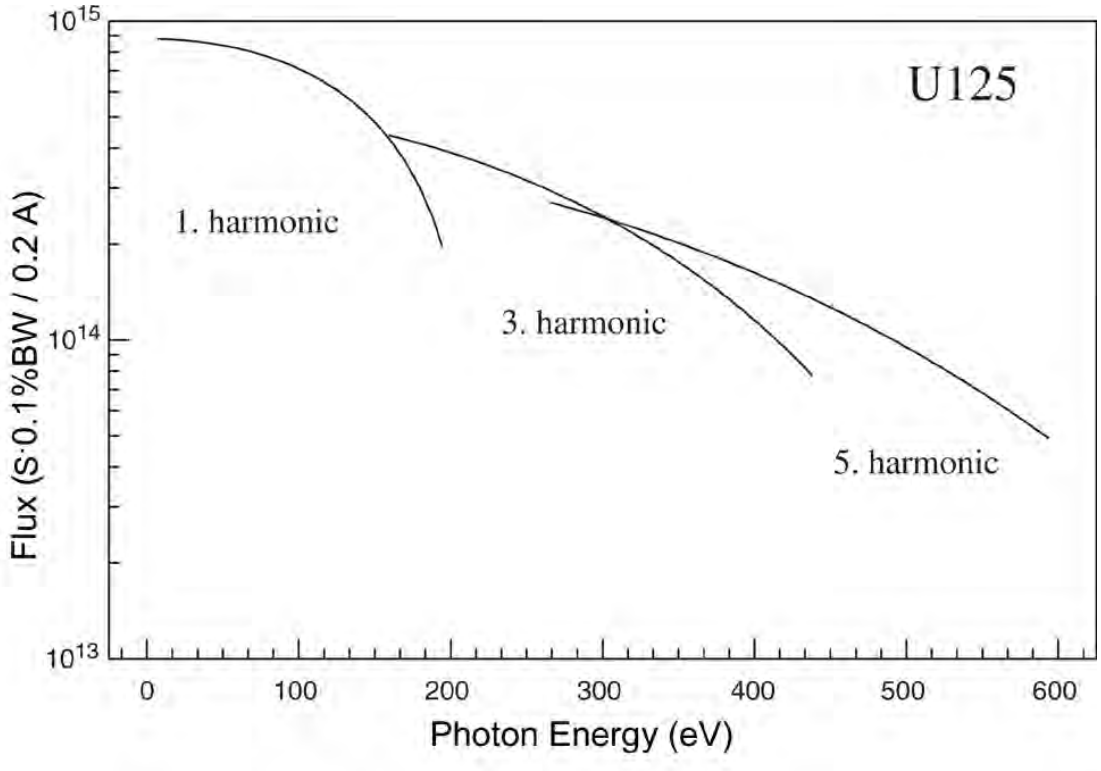

Figure 2.4: Photon flux of the undulator U125/1 for 200 mA ring current as a function of photon energy.

Spherical Grating Monochromator (SGM)

The measurements and the preparation on vanadium dioxide (VO_2) films on a TiO_2(110) crystal, presented in this work in Chapter 3 have been performed at the MBI-BESSY beamline U125/SGM. Monochromators employed in the soft X-ray region of synchrotron radiation use reflective gratings to select a certain band pass of wavelengths λ out of the emitted spectrum. This is based on the grating equation:

$$\sin\theta_i + \sin\theta_d = m\lambda N, \tag{2.12}$$

where θ_i and θ_d are the incident light and diffraction angles, m is the diffraction order and N corresponds to the line density. The light is diffracted under different angles for different wavelengths and thus it is possible to select the desired photon energy. An important parameter is the resolving power $R = E/\Delta E$, describing the energy spread ΔE around the central energy E=hc/λ.

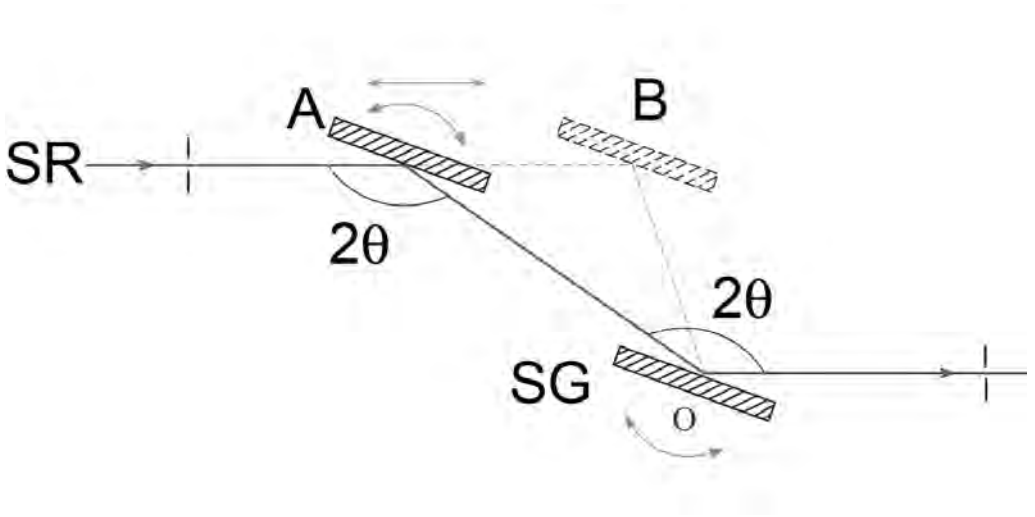

Figure 2.5: Principle of the MBI spherical grating monochromator at BESSY (Undulator U125). Incoming SR-light (from left) hits a rotatable gold coated plane mirror with extremal positions (A) and (B). It is then deflected in the center (O) of the spherical grating by 2θ.

The monochromator used at the MBI-beamline U125/1-SGM was a spherical grating monochromator (SGM), operating in the range between 20 and 180 eV with a resolving power of 6000. Figure 2.5 illustrates the setup of the monochromator optics. The monochromator construction is based on the variable included angle (VIA) principle. The grating chamber contains two spherical gratings, which may be used in alternation. The first grating has 700 lines/mm, and is optimized for photon energies between 20 to 50 eV; the second grating, with 1666 lines/mm

covers the 50 to 180 eV photon-energy range. The gratings can be moved in and out of the optical path under vacuum conditions. To change the transmitted wavelength the grating and the mirror inside the monochromator have to be rotated and positioned according to trajectories, which were determined by ray tracing calculations. Synchronized with these movements the undulator gap has to be adjusted. Using the 1666 lines/mm grating with a 200 μm entrance slit at 64 eV photon energy and 0.1 A ring current, the photon flux at the sample was determined to be approximately $4 \cdot 10^{12}$ photons/$(s \cdot 0.1\%\text{BW})$ with an enery resolution of about 100 meV.
The synchrotron radiation spot at the sample position was elliptical in shape with a size of 1×0.3 mm on a plane perpendicular to the beam.

2.2.2 Endstation at the MBI-beamline U125/1-SGM

To study the metal-semiconductor phase transition in vanadium dioxide films (VO_2), we need to prepare and handle films under ultrahigh vacuum UHV conditions. Preparation and measurements were done in a multi chamber ultrahigh-vacuum apparatus with a base pressure around $2 \cdot 10^{-10}$ mbar. The system consists of an interconnected load-lock, preparation and analysis chamber, and a manipulator for sample transfer and handling. Each chamber is independently pumped and may be separated by valves. A schematics of the apparatus is given in Fig. 2.6.

The load-lock uses a magnetic transfer rod that allows storage of up to three samples. The typical working pressure in this chamber is 1 to $5 \cdot 10^{-8}$ mbar.
The preparation chamber contains standard surface tools: a 4-grid LEED/AES system (ErLEED 3000D, Vacuum Science Instruments), an IS 2000 ion sputter gun (Vacuum Science Instruments), and a quadrupole mass spectrometer (Balzers, QMS 421) that can be used for the analysis of molecules with masses up to 2048 amu. A standard evaporator (Oxford scientific) is mounted to allow deposition of vanadium, and a gas-inlet system is available to dose oxygen. As illustrated in Fig. 2.7 the VO_2 sample was mounted on a Tantalum plate with slits both held by two Tantalum clamps. Two Tungsten wires of 0.25 mm diameter fix the sample onto the holder. Thermocouples of type K were attached between the sample and the Ta-plate to ensure a good temperature measurement. The Tungsten-wires, which are in thermal contact with the sample, were used to heat the sample. The holder has two Molybdenum-plates mounted in the same plane as the sample, which were covered with fluorescent material to optically detect synchrotron light (60 eV) and laser light (1.56 eV) and find the spatial overlap between laser and synchrotron beams. The sample is in thermal contact to a LN_2 reservoir, which can be heated using resistive heaters (thermocoax). This allows for photoemission measurements at variable temperature between 100 and 420 K. The sample holder is mounted on a horizontal manipulator, which could be moved into the two separated chambers. Figure 2.6

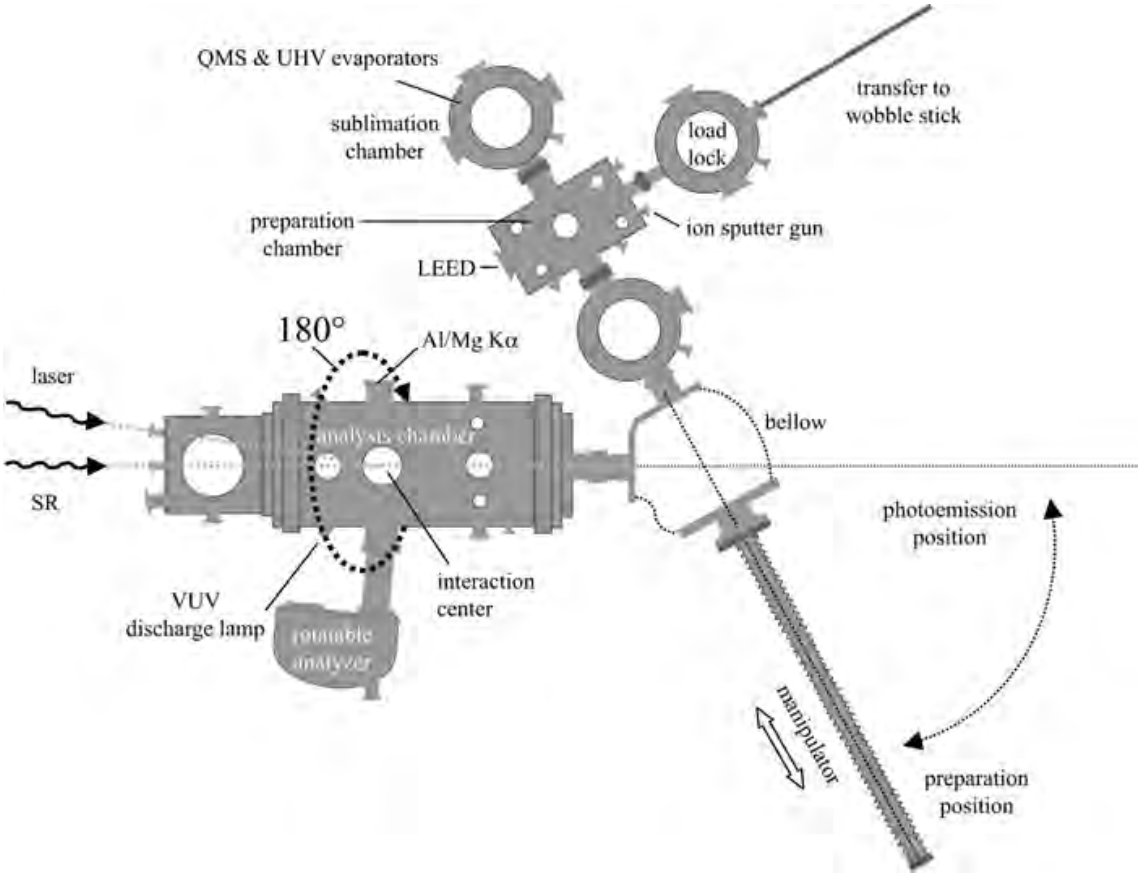

Figure 2.6: Layout of the MBI UHV surface apparatus for combined experiments with laser and synchrotron radiation. Photoemitted electrons are analyzed in an hemispherical electron analyzer.

illustrates the two extreme positions of the manipulator. Besides an azimuthal rotation around the surface normal can be tilted by up to 90°. This flexibility ensures that practically every desired position and orientation of the sample with respect to the incident synchrotron radiation can be realized.

The analysis chamber is rotable around the axis of the synchrotron beam by a servomotor. Thus the emission angle relative to the synchrotron polarization can be varied. The entire analysis chamber has a 1 mm μ-metal shielding that shields the earth's magnetic field to less then 0.1 μT at the sample position. The chamber is equipped with a hemispherical electron energy analyzer (Omicron EA 125 U5), which will be described in detail in Section 2.2.5. The experimental setup also contains an X-rays source (Omicron DAR 15) with Al and Mg twin-anode, and a VUV discharge lamp (Omicron, HIS 13). A CCD camera attached to one of the windows provides an image of the sample inside the analysis chamber.

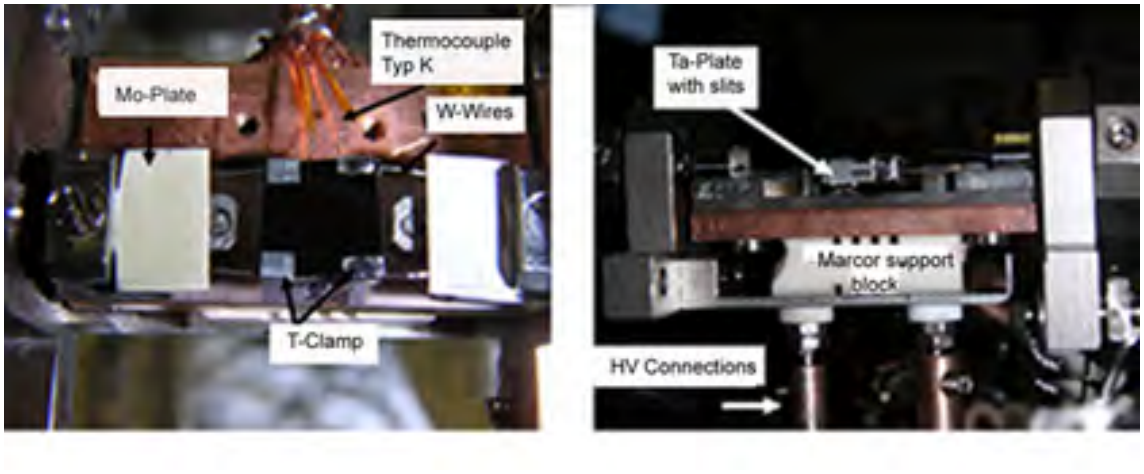

Figure 2.7: View of the VO_2 sample holder, from the side (left picture) and the top (right picture).

The laser system used for combined experiments with laser and synchrotron was a Vanadat laser (Nd:YVO_4) with a pulse duration of 14 ps, fundamental wavelength (λ=1064 nm) and 1.25 MHz repetition rate (for details see reference [Brö04]). This laser system with low repetition rate together with the large focus of the SR beam made two-photon photoemission experiments impracticable. To solve this problem, we needed to improve the laser system to obtain higher fluence. We moved to another monochromator, to obtain a smaller focus and thus a higher number of probe photons per pulse.
Further requirements for two-photon photoemission experiments using laser and synchrotron radiation are discussed in Appendix A.6.

2.2.3 Beamline U125/1-PGM

Since March 2004 the MBI experiments with combined laser and synchrotron radiation are relocated to the plane grating monochromator [Fol98] U125/1-PGM beamline at BESSY. The move included several modifications of the photoemission endstation, (Section 2.2.4), and the re-design of the present refocusing chamber improving the spatial overlap between laser and synchrotron radiation and also including an optimal laser light-path.
This beamline offers photon energies ranging from 15 to 600 eV, and provides a micro focus for efficient two-photon pump-probe experiments. Figure 2.8 illustrates the layout of the U125/1-PGM beamline.

The major advantages of this beamline with respect to the U125 (SGM) are the larger range of photon energies increasing the SR intensity and a micro spot shown in Fig. 2.9. The PGM uses an old optical principle: the illumination of a plane grating with collimated light and is based on a variable deviation angle. The plane mirror M2

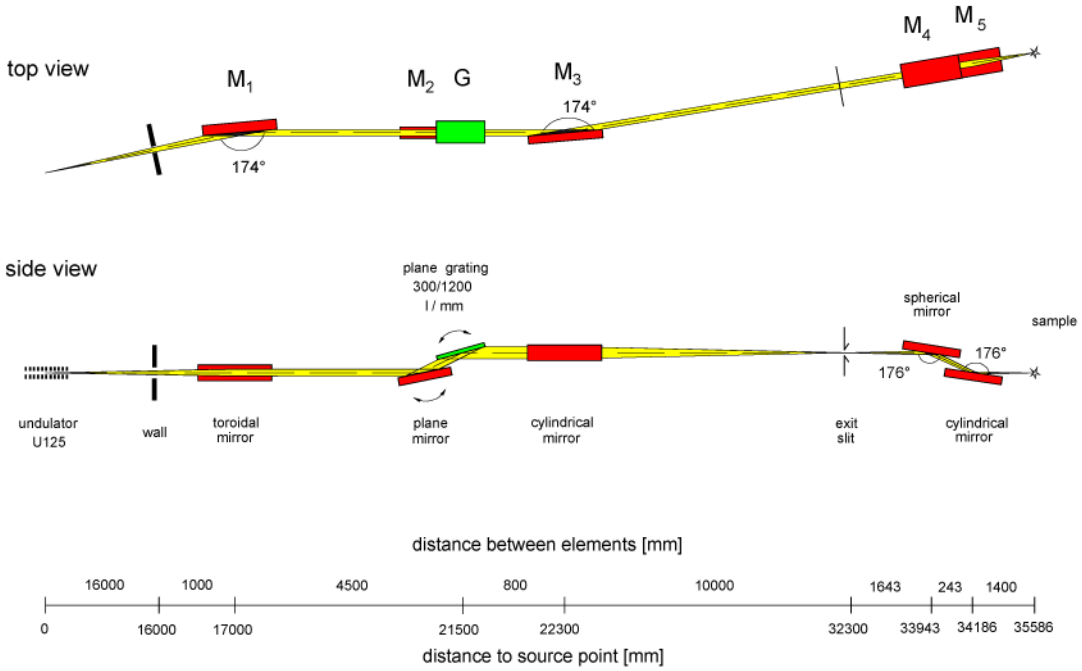

Figure 2.8: Sketch of the U125/1 Plane Grating Monochromator (PGM) beamline (top and side view). The main components of the monochromator are: M1, a toroidal mirror which collimates the light in the horizontal and vertical directions. The plane mirror M2 is used to vary the deviation angle at the plane grating G. Vertically, the diffracted light is focused onto the exit slit by the cylindrical mirror M3. The refocussing into the endstation is performed by the mirrors M4 and M5 in the vertical and horizontal directions, respectively.

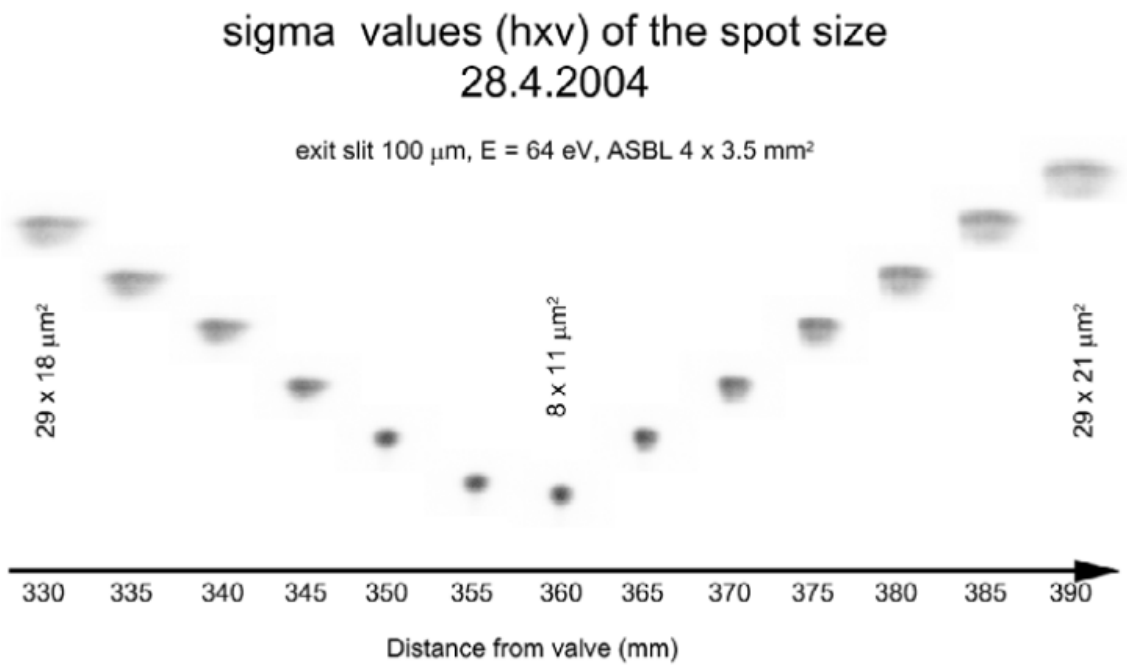

Figure 2.9: Change of the spot size as a function of the distance to the last valve from the beamline for a photon energy of 64 eV and 100 μm exit slit.

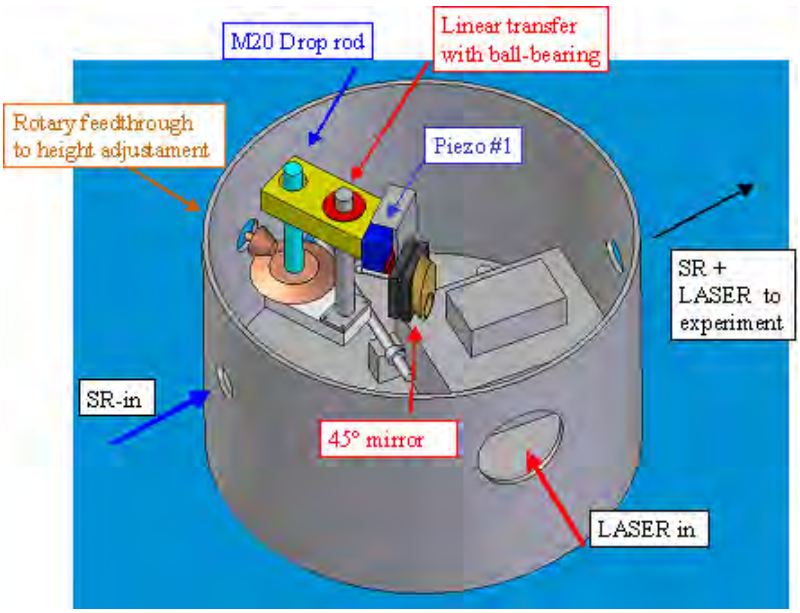

Figure 2.10: Layout of the re-designed refocussing chamber with improved overlap between the synchrotron and the laser beam.

is used to vary the deviation angle at the grating, (Fig. 2.8). The monochromator is equipped with two laminar gratings with 300 and 1200 lines mm^{-1} covering the energy range from 20 to 600 eV. Because of the high heat load, the mirrors M1 and M2 as well as the gratings are water cooled via copper blocks. The PGM operates without an entrance slit because the undulator source is highly collimated. The photon flux can be measured by detecting the photoelectric current from a gold-mesh or a photodiode placed directly after the refocussing optics. Figure 2.10 illustrates the laser path in the new refocussing chamber. The overlap between the nearly collinear laser and synchrotron beams is significatively improved. An additional plane mirror has been added to the refocussing chamber between the two refocussing mirrors for nearly collinear laser and synchrotron alignment. Laser and synchrotron beams are reflected to the endstation coplanar enclosing an angle of 7^o. The plane mirror is movable to adjust its height and the angle incident.

2.2.4 Endstation at U125/1-PGM

The photoemission endstation consists of a two-chamber UHV system depicted in Fig. 2.11. Both are independently pumped and connected by a gate valve. The preparation chamber contains the surface tools already mentioned in Section 2.2.2. The analysis chamber is equipped with a 125 mm mean radius hemispherical electron analyzer (EA 125, Omicron) with a five channel detector (Section 2.2.5).
The analysis chamber can be rotated around the axis of the synchrotron beam by a servo motor. A complete re-design of the chamber mounting was necessary to adopt the endstation to the U125 PGM beamline. The feet of the chamber are air cushioned to adjust height and horizontal position of the endstation to the beamline. A horizontal manipulator is mounted for translating the sample along both chambers. This manipulator contains a He-cryostat for cooling with Helium or Nitrogen and an electric heat exchanger. A thermocouple type K is attached to control the temperature of the sample. The manipulator is additionally rotable by 360^o around its main axis. The vertical and horizontal movements are controlled by two micrometer screws. Figure 2.12 shows a front and a side view of the silicon sample holder. The tilt angle of the sample is changed by the rotatable copper screw.

2.2.5 Electron Analyzer

Figure 2.13 illustrates a schematic representation of the Omicron EA125 analyzer. The hemispherical analyzer consist of three different sections, the electrostatic input lens, the hemispherical dispersive elements and the detector. Each section will be explained in detail below.

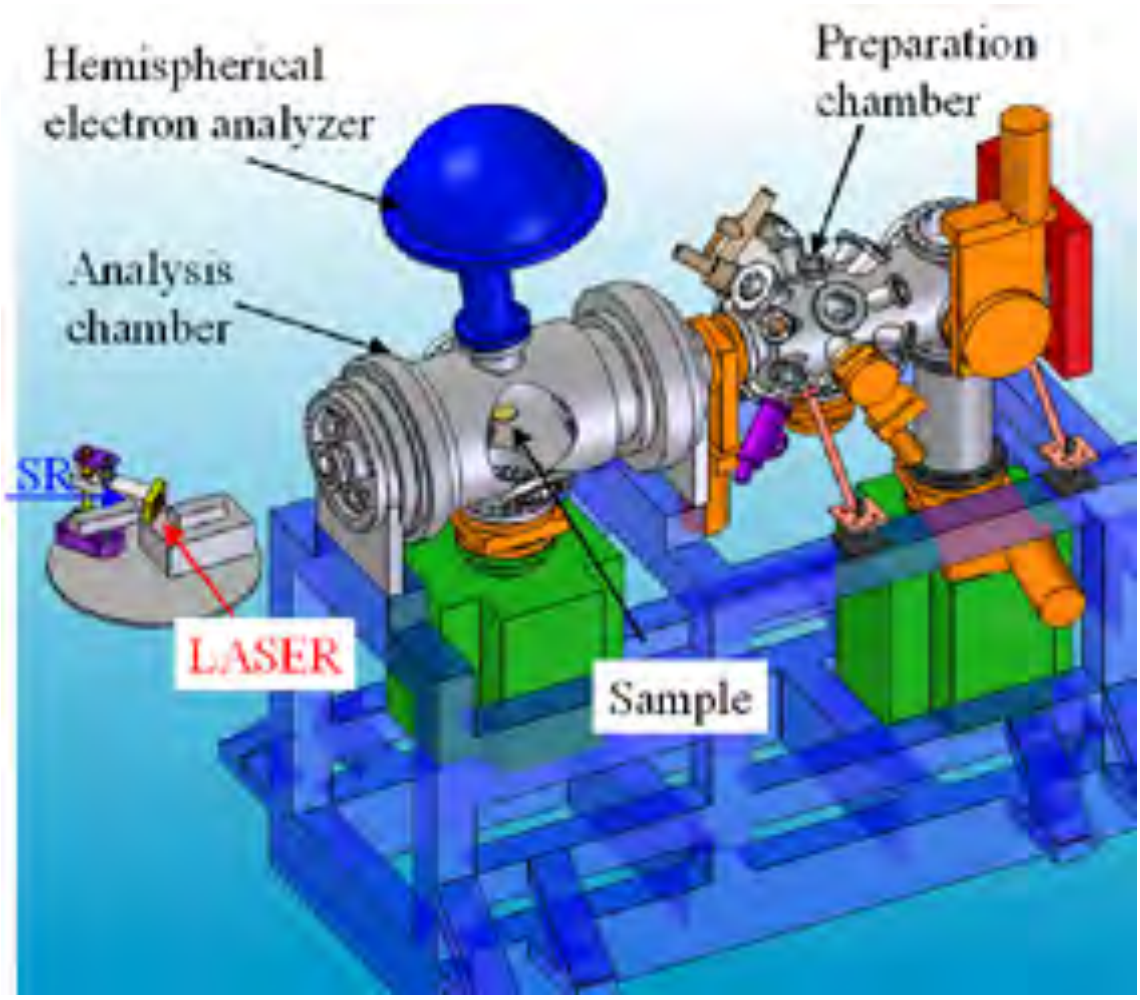

Figure 2.11: Schematics layout of the UHV equipment.

Universal Lens

The electrostatic lens system focuses the photoelectrons from the sample onto the entrance slit of the hemispherical analyzer. The lens system can be divided into two parts. The first stage of the lens system, *the magnification lenses*, are used to adjust the spatial and angular resolution of the analyzer. These magnification lenses are indicated in Fig. 2.13 by the numbers 1, 2 and 3. Each number corresponds to a magnification mode. The magnification is changed by applying a certain potential to the chosen lens connecting the remaining lenses to ground.
In the high-magnification modus, number 1 in Fig. 2.13, the focussing voltages run proportional to the electron kinetic-energy. The electrons are strongly accelerated with a low angular resolution of $\pm 8^{\circ}$ and a focal size on the sample of approximately 1 mm diameter.

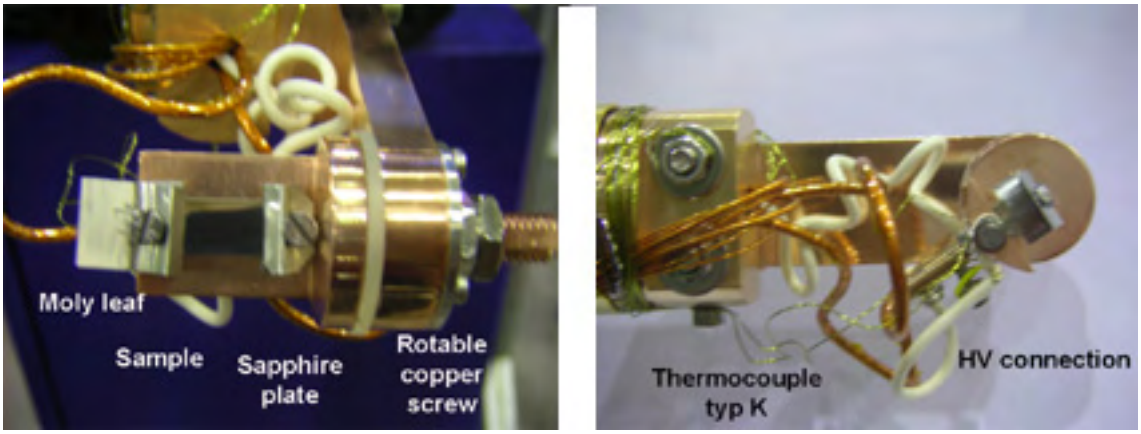

Figure 2.12: Silicon sample holder, front and view side to the left and right.

In the low-magnification modus the emitted electrons are collected with high angular resolution of $\pm 1^{\circ}$ and a large focal size of approximately 3 mm.
In the medium-magnification modus is in between low and high magnification.
The second stage of the lens system, (lens 4 to 6, in Fig. 2.13), is used to retard the photoelectrons and adjust their kinetic energy to the desired pass energy of the hemispherical analyzer. A non-adjustable aperture at the end of this lens is put at the position of maximum electron transmission. This aperture stops the most aberrated electrons and serves for predefining the probed area on the sample.
The transmission is independent of the kinetic energy of the electrons. The zoom lens-stage images the electrons from the aperture of the first lens onto the entrance slit of the hemisphere. An angular defining aperture is positioned at the entrance of the hemisphere [Omi].

Hemispherical Dispersive Element

The energy filtering takes places in the hemisphere of the analyzer. Between the inside and outside hemisphere a voltage $V_{1,2}$, is applied, which generates an electric field proportional to $1/R^2$. The photoelectrons will experience a centripetal force and hence undergo uniform circular motion. The radius of curvature is determined by the electron velocity, which is directly related to the kinetic energy.

$$e(V_2 - V_1) = E_{kin}(\frac{R_2}{R_1} - \frac{R_1}{R_2}) \tag{2.13}$$

where V_1 and V_2 are the voltages on the inner and outer hemisphere with radii R_1 and R_2, respectively. The voltage applied at the inside and outside hemisphere are:

$$V_1 = E_{pass}(2\frac{R_o}{R_1} - 1) \quad V_2 = E_{pass}(2\frac{R_o}{R_2} - 1) \tag{2.14}$$

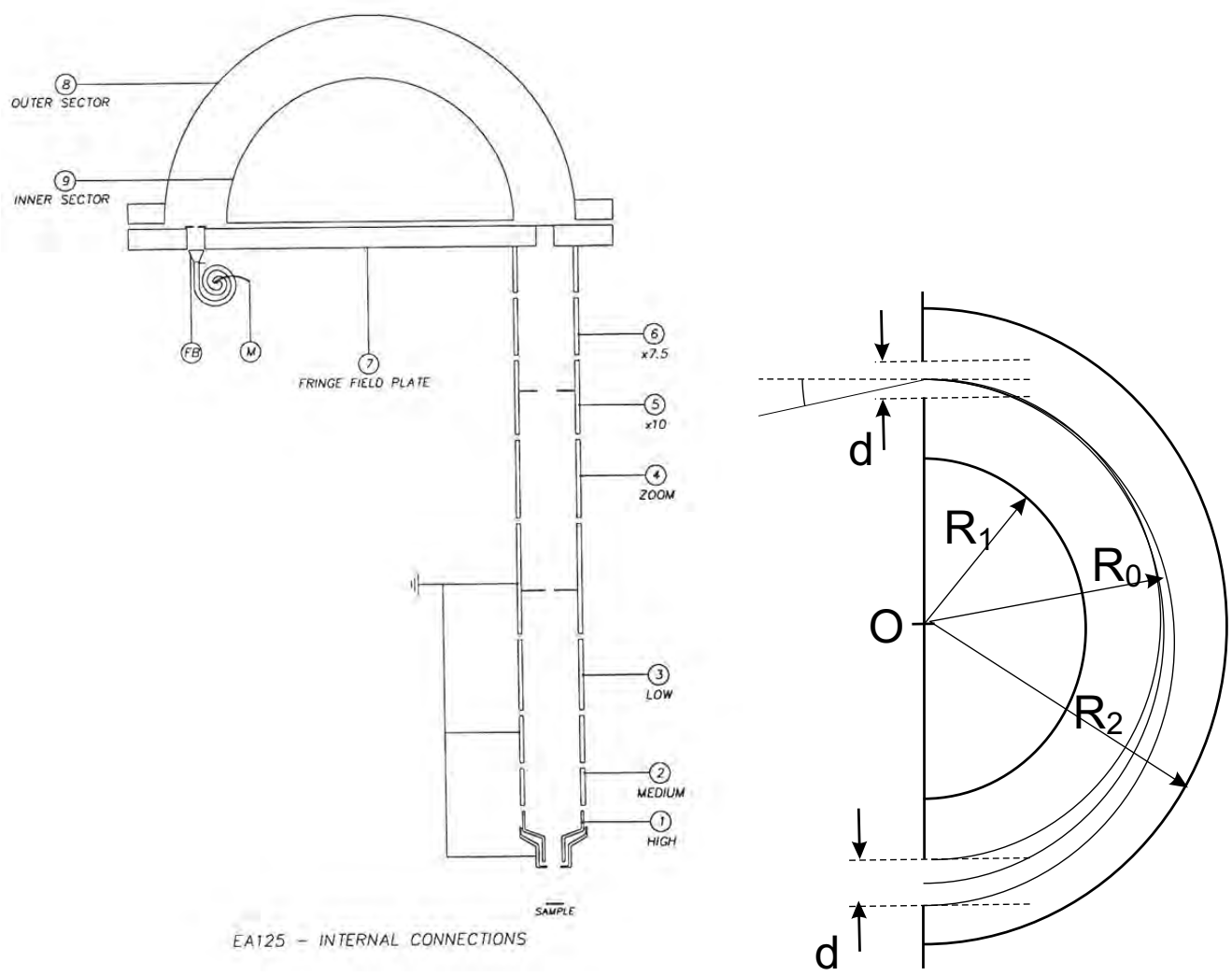

Figure 2.13: Schematic of the hemispherical analyzer EA 125 (Omicron). To the left the complete setup of the lens system, the hemispherical analyzer, and the detector is shown. To the right the path of the electrons inside the hemispherical analyzer is depicted. R_1 and R_2 denote inside and outside radius, R_0 is the radius defining the pass energy of the electrons for certain applied potentials at the hemispheres and fringe-field plate.

for the desired pass energy E_{pass}. R_o is the mean radius of the hemisphere. Both voltages are referenced to the entrance and exit slit potential, which is called the retard potential V_R. The retard potential is used to filter kinetic energies of the electrons generated by photoemission. The analyzer with an energy E_{pass}, transmits electrons for the chosen pass energy and filters out the rest of electrons so that $eV_R = E_{Kin} - E_{Pass}$. Five channeltrons detect several kinetic energies in parallel. The energy resolution of the analyzer is given by [Omi]:

$$\Delta E = E_{pass}(\frac{d}{2R_0} + \alpha^2) \tag{2.15}$$

where d is the sum of entrance and exit-slit widths and α is the angle of incidence at the entrance-slit of the analyzer (see Fig. 2.13).
For the EA 125 the focussing angle is 3° and the mean radius R_o amounts to 125 mm. Entrance slits widths of 1, 2, or 6 mm are available. For the exit slit, four arrays of size 6 × 12 mm, 4 × 12 mm and 1 × 12 mm can be selected. With the largest exit slit the five channeltrons are covered. For 5 eV pass energy and 6 mm slits, the energy resolution ΔE is 0.12 eV. In photoemission usually the pass energy remains fixed and the measurement of the kinetic energy of the photoemitted electrons implicitly demands a change to the retard potential. As the retard potential is a constant portion of the kinetic energy of the electrons, the retard ratio k is constant:

$$k = \frac{R + E_{pass}}{E_{kin}} \tag{2.16}$$

However, throughout the scan range the transmission of the analyzer continuously varies the transmission factor, for the CAE (constant analyzer energy) measuring mode is given by [Ruf00]:

$$T = \frac{E_{pass}^2}{E_{kin}} \tag{2.17}$$

2.3 Laser Setup and Synchronization Scheme

Time-resolved pump-probe experiments with a combination of laser and synchrotron radiation require the synchronization of two independent light sources being the most demanding part of the present experiment. Furthermore, the repetition rate, the fluence and the wavelength of both sources is quite different.
This section will present the improvements of the laser system including femtosecond pulse width, pulse amplification and an effective micro focussing. A new laser system was prepared for the U125/1-PGM beamline and is in operation since May 2004.
In this section we will describe the necessary steps to start measuring; synchronization, adjusting temporal and spatial overlap, gating the photoemitted electrons and

their detection.

2.3.1 Synchronization of Laser and Synchrotron

The combined laser and synchrotron experiments require that the repetition rate of both light sources match. Table 2.1 presents an overview of the different operation modi and repetition rates of the synchrotron probe-pulse. The spot size of the probe pulse on the sample is approximately 50 μm (Fig. 2.17) and the available photon energies range from 20 to 600 eV.

Operation Mode	Repetition Rate (MHz)	Pulse Duration (ps)	$N_{Bunches}$	I_{max}(mA)
Multibunch	500	50-100	350	260
Hybrid	1.25	50	1	10
Single Bunch	1.25	30-80	1	20
Low-alpha	500	5-15	350	40

Table 2.1: Operation mode of BESSY with pulse duration, repetition rate, the number of bunch, and the maximal current on the ring.

A regenerative amplified Ti:sapphire laser (Coherent, RegA9050) is used as pump source, producing pulses width of 70 fs duration at a repetition rate of 208.3 kHz. The pulse energy at the fundamental wavelength of 800 nm is 6 μJ, second harmonic generation is available. The focal diameter is about 70 μm as illustrated in Fig. 2.17.
The new laser system and the synchronization electronics is sketched in Fig. 2.14, the colors represent the different contributions:

- blue color show the regenerative amplifier (Reg A, Coherent)
- red color represent the main clock of the radio-frequency (RF) cavity from BESSY at multibunch (500 MHz) and singlebunch (1.25 MHz)
- green part are the home-built seed laser and the electronic of the synchronization, which was developed at the Max-Born Institut. The 500 MHz BESSY masterclock is divided by 6 generating the 83.3 MHz RF signal used for synchronization of the seed laser via a phase detector. The 1.25 MHz BESSY bunchmarker divided by 6 is used to trigger the Reg A controller with a repetition rate of 208 kHz and to reset the feedback electronics.

The seed laser is a home-built Ti:Sapphire oscillator (Fig. 2.15). The repetition rate is 83.3 MHz (12 ns period), which coincides with every sixth synchrotron-radiation

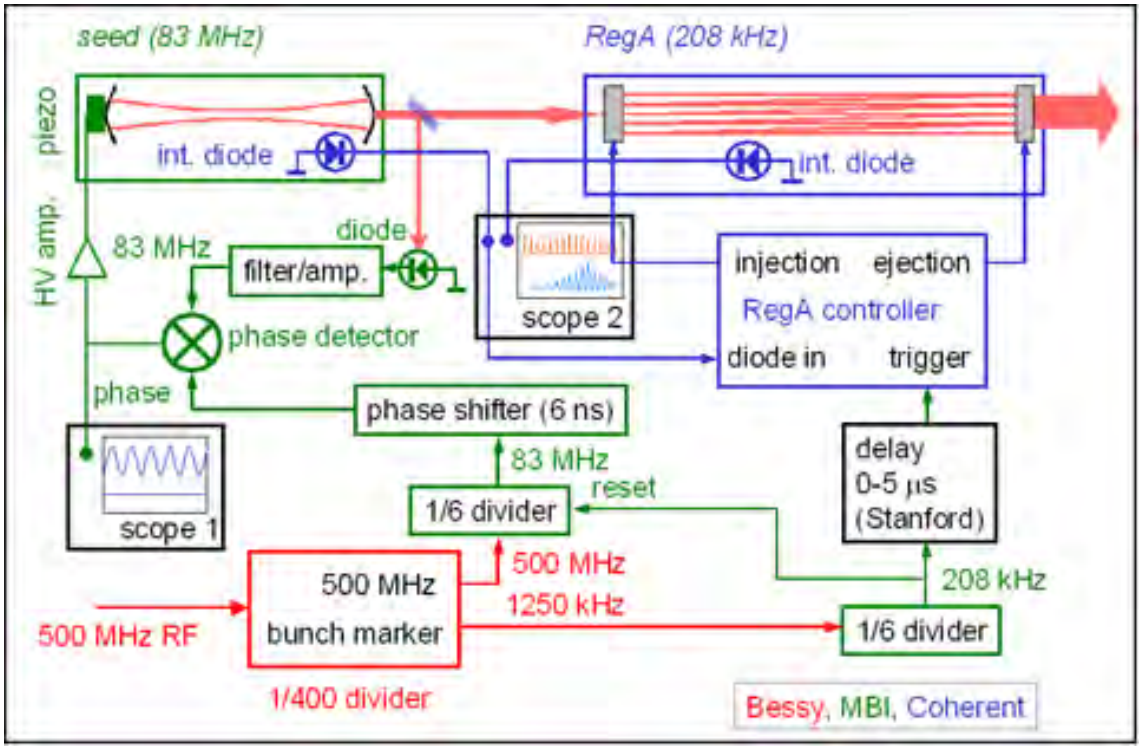

Figure 2.14: Synchronization scheme of the regenerative amplified Ti:Sa system.

pulse at BESSY in multibunch operation-mode. Synchronization is done by dividing the 500 MHz (2 ns period) master clock from BESSY by 6 and comparing the phase of this sinusoidal 83.3 MHz signal to the phase of the laser measured by a photodiode.
The cavity length is controlled by mounting one of the end mirrors on a piezo crystal. The piezo controls the cavity lenght and therefore the oscillator frequency. The control signal of the phase detector steers the resonator length by a fast feedback loop. The seed pulses pass through the stretcher and are amplified in a regenerative amplifier (RegA). Afterwards the pulses are compressed and directed to the experiment. The output couples of the regenerative amplifier is triggered by every sixth bunch-marker pulse (1.25 MHz), which matches exactly the 208.3 KHz repetition rate of the amplifier system. At this stage pump-laser and probe-synchrotron pulses are synchronized with a jitter better than 5 ps. The temporal alignment of laser and synchrotron pulses is achieved by an electronic delay with an accuracy of 5 ps. The electronic delay (phase shifter) are necessary to select the right seed pulse and to fine-adjust the seed relative to the synchrotron light.
The RegA-controller triggers the *injection/ejection* mechanism not only via the trigger input, but also follows the signal from photodiode of the seed laser. Oscilloscope 1 displays the output of the phase mixer.

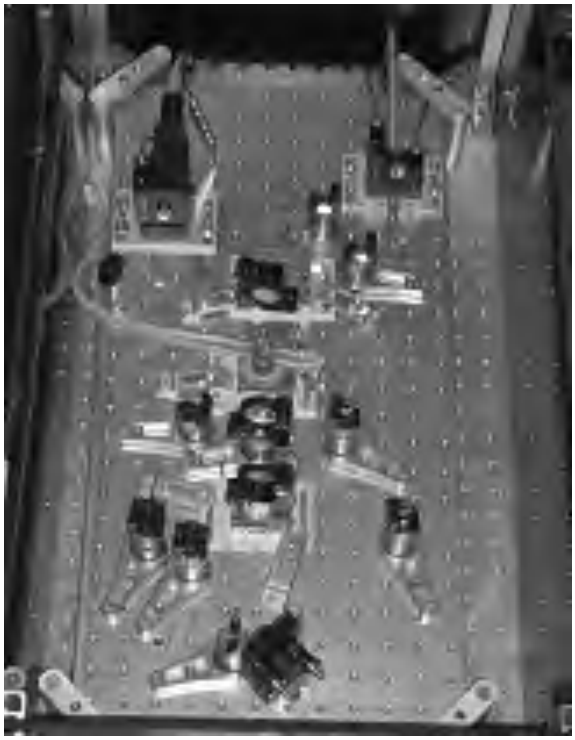

Figure 2.15: Home-built Ti:Sapphire oscillator with a repetition rate for 83.3 MHz.

The delay generator uses the frequency input of 208 kHz as start signal. One output from the delay generator leads to the external trigger from the RegA controller. The second one supplies the start signal for the measurement to detect the "correct" synchrotron bunch, which coincides with the laser pulse. The third one supplies the electronic signal to gate the photoemitted electrons. Hereafter, we will firstly explain the overlap, i.e., detecting the temporal and spatial positions of the laser pulse with respect to the synchrotron pulse. Then we describe how the electronic gate is set. Finally we illustrate the detection and analysis of the electrons photoemitted from the sample.

2.3.2 Temporal and Spatial Overlap

After the laser pulse leaves of the RegA, the beam passes the variable attenuators, a telescope system and a focussing lens system with 2 m focal length, focussing the beam onto the sample positioned in the analysis chamber. The position of the laser-beam is adjusted by moving a step motor sustaining the lens. The lateral position of the laser spot can be adjusted with a precision of approximately 2 μm. The laser beam is steered into the refocussing chamber of the beamline through a fused silica viewport (Fig. 2.10). Both beams enter the analysis chamber being nearly collinear

Figure 2.16: Signal of both laser and synchrotron pulses (in multibunch mode) on a fast photodiode monitored by a fast sampling oscilloscope (500 MHz bandwidth).

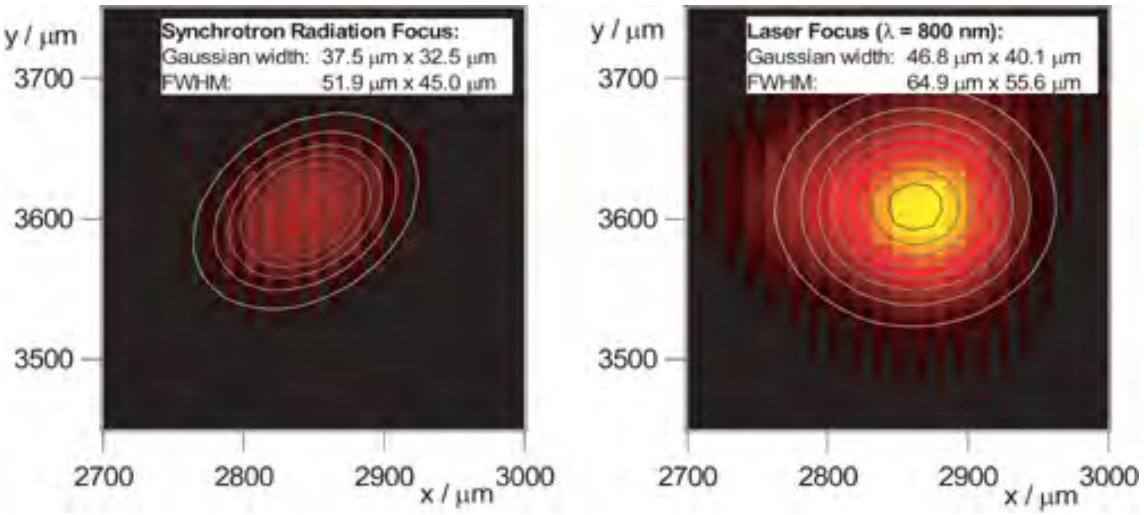

Figure 2.17: Images of the fluorescence and stray light from the synchrotron and laser beam, respectively.

enclosing an angle of 7°. When the synchronization between laser and synchrotron is working, the laser pulse coincides with each sixth synchrotron pulse. The time delay between laser-pump and SR-probe pulse is detected using a fast XUV sensitive photodiode inserted at the position of the sample the accuracy of this procedure is

50 ps. Figure 2.16 shows the signal from the fast photodiode of both the laser and SR pulses (in multibunch mode) monitored by a fast sampling oscilloscope (500 MHz bandwidth). The temporal position of the laser pulse is adjusted by an electronic delay.
The spatial overlap of laser and SR beam is monitored using a CCD camera. For this purpose a fluorescent plate is mounted on the sample holder coplanar with respect to the sample surface. The spatial resolution of this setup is limited by both the grain size of the fluorescent material and the imaging system to approximately 7 μm. Figure 2.17 shows images of the fluorescence and stray light of the synchrotron and laser, respectively. The size of both spots is about 20 to 50 μm.

2.4 Electron Detection

The present section explains the modified electronics of the analyzer for time-resolved photoemission spectroscopy at a certain kinetic energy. A time resolving and energy dispersing photoelectron detector has been set up for pump-probe photoemission spectroscopy. The time resolution of the detector is 1 ns and allows an assignment of the photoelectron signal to a specific synchrotron radiation pulse for any filling pattern of 3^{rd} generation synchrotron storage rings. This leads to an overall time resolution only limited by the probe-synchrotron pulse width, which changes for the different operation modes of the synchrotron facility (Table 2.1). The hemispherical analyzer is already described in Section 2.2.5. A sketch of the experimental setup for time- and energy-resolved photoelectron spectroscopy is given in Fig. 2.18 and details of the electronic detection are shown in Fig. 2.19. Photoelectrons from the sample are focussed by a lens system onto the entrance slit of the hemispherical analyzer. The electrons with a kinetic energy defined by the mean retarding potential and the analyzer pass-energy reach the exit slit and are detected using five channeltron electrons-multipliers.
The resulting electron pulses (single electron counting) with a rising-edge of $\approx$ 5 ns and an amplitude of 2 mV are decoupled from the high voltage of the channeltron multipliers. The pulses are preamplified via home-built 250 MHz bandwidth preamplifiers by a factor of 10 and discriminated via constant fraction discriminators (CFD, 454, Canberra, Meriden, USA) with a time resolution of approximately 60 ps. The normalized pulse from the constant fraction discriminator is fed as a stop signal in a time-to-digital converter (TDC, GPTA, Berlin, Germany). The TDC, which has a time resolution of approximately 180 ps is triggered by the electronic bunch-marker signal provided by the SR storage ring. The bunch-marker signal has a frequency of 1.25 MHz, which corresponds to the roundtrip frequency of a single electron bunch in the storage ring [Gie03].
In this scheme, denoted multiprobe mode [Wid03], a laser-excited state is probed by consecutive pulses in multibunch mode. Zero delay is now determined recording the

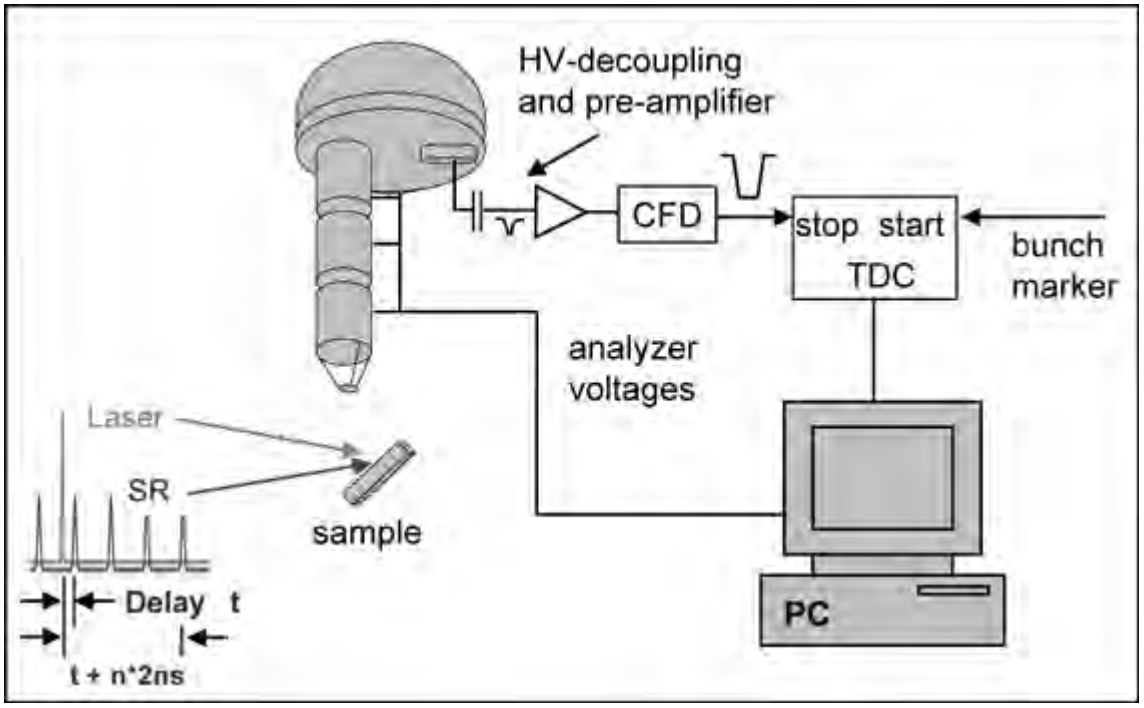

Figure 2.18: Setup for time- and energy-resolved photoelectron spectroscopy.

laser-induced photovoltage on silicon. This can be done by timing the analyzer energy to, e.g, the edge of the Si 2p core-level signal. The photovoltage shifts the Si 2p peak into the analyzer energy-detection-window and the count rate increases. This is illustrated in Fig. 2.21a. Without laser the time of flight photoelectron spectrum simply resembles the filling of the storage ring with a period of 800 ns; 350 bunches with 2 ns interval are separated by a $\sim$ 100 ns gap (blue-spectrum). With the laser on the surface photovoltage shifts on the Si 2p core-level into the detection window and leads to an increase of the count rate (red-spectrum). Recording the time of flight spectrum we detect both the increase and the decay of the photovoltage.

The data show in Fig. 2.21 have been measured in low-α hybrid mode. In this hybrid mode a single electron bunch is injected in the storage ring in the 100 ns gap between multiple electron bunches. This isolated bunch is used for time-resolved spectroscopy.

Using the fast photodiode the laser pulse and the SR hybrid pulse are overlapped in time with an accuracy of about 50 ps. Since the roundtrip frequency of the hybrid-pulse of 1.25 MHz is six times larger than the laser repetition rate of 208.3 kHz we identify the probing hybrid bunch by the above described multiprobe mode. Than an electronic gate is set to solely count electrons excited by the probing hybrid bunch (green-line in Fig.2.21). As already mentioned, the gate is set by the delay

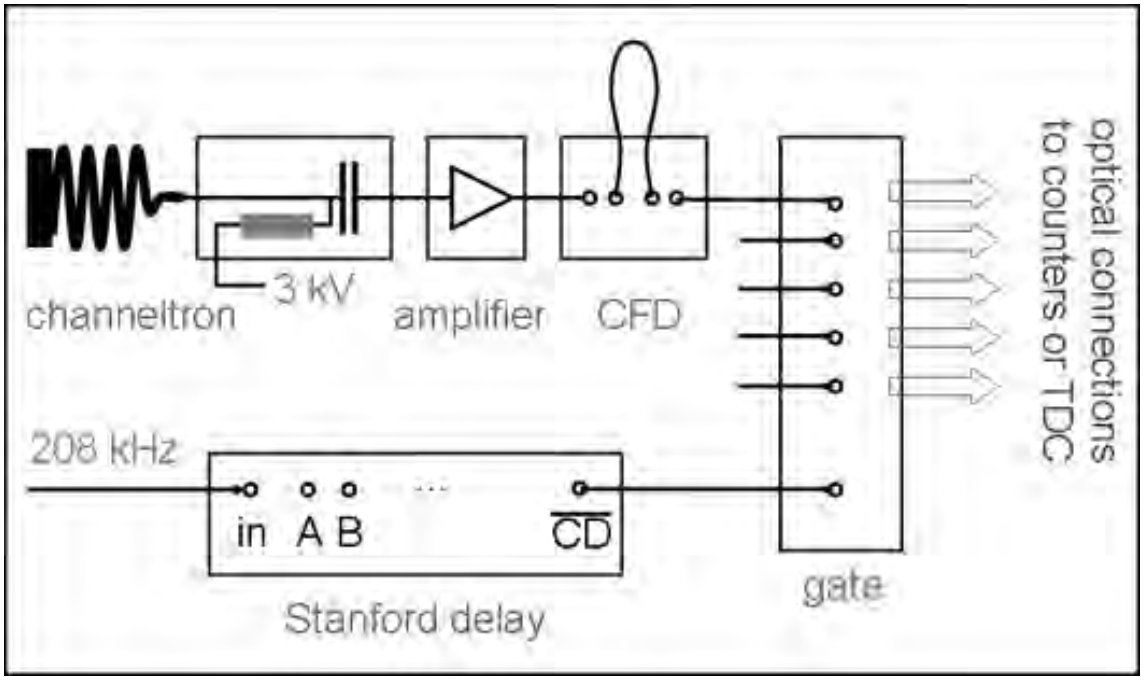

Figure 2.19: Setup of the experiment for time- and energy-resolved photoelectron spectroscopy.

generator, which also triggers the ejection of laser pulses out of the amplifier (see Fig. 2.19).
The delay between laser and synchrotron pulse in a time-resolved measurement is now controlled electronically by computer-controlled phase shifter, which shifts the phase of the 83 MHz signal derived from the 500 MHz master clock with respect to the phase of the seed laser.
The complete timing procedure is summarized in Fig. 2.20. Once laser pulse and hybrid or single bunch derived SR pulse overlap, a time of flight spectrum is recorded. The above described scheme also works for single bunch mode. This allows to identify the relevant event by, e.g, the increase of the recorded photoemission signal.
The delay of the electronic gate Δt_{gate} is determined by the delay between bunch marker and synchrotron pulse Δt_2 and the time of flight Δt_{TOF} of the photoelectrons. The latter depends on the pass energy of the analyzer. We note that the above approach only works if the duration of the processes to be investigated is smaller than a few nanoseconds. For a reasonably high transmission and energy resolution of the analyzer the time spread of the photoelectrons in the analyzer amounts to about 40 ns. Hence, photoelectrons for one particular SR pulse can be singled out only in single bunch mode or in hybrid bunch mode. The experiments described in Chapter 4 prove that the overall time resolution is below 10 ps.

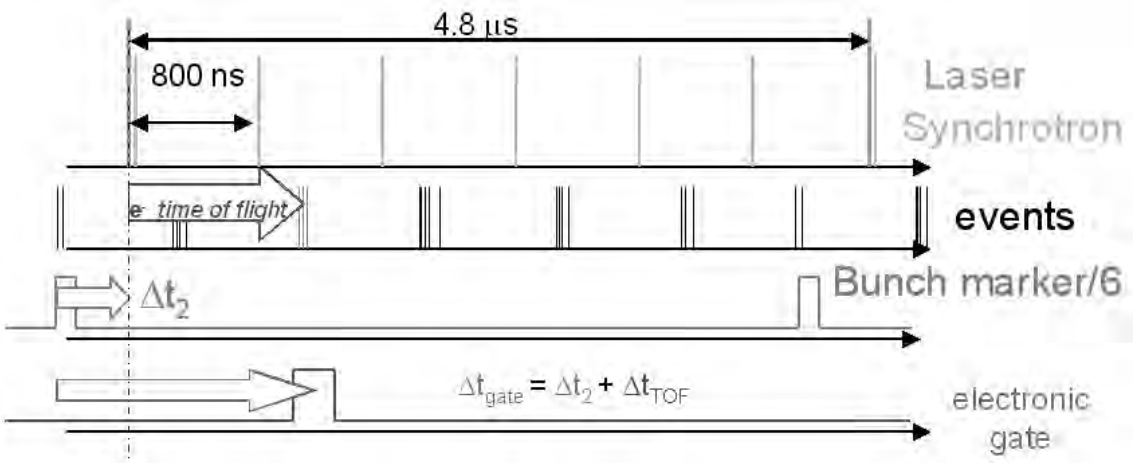

Figure 2.20: Timing of the pump-laser and synchrotron pulses with the photoemitted electrons (TOF) and the electronic gate.

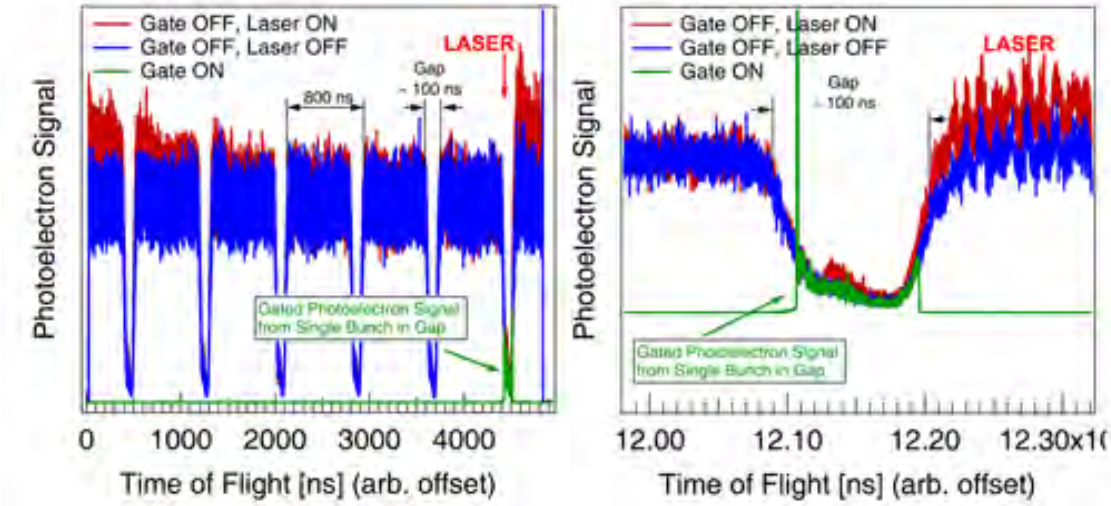

Figure 2.21: Time of flight photoelectron spectra for hybrid bunch mode with (green) and without electronic gate (red and blue). Right: A zoom of the gated photoemission signal.